Terr. Atmos. Ocean. Sci., Vol. 20, No. 1, 237-250, February 2009 doi: 10.3319/TAO.2008.01.22.01(F3C)

Campaign Investigation of Ionospheric Plasma Irregularities in Sporadic E Region Using FORMOSAT-3/COSMIC Satellite and Chung-Li 30 MHz Coherent Radar

Chien-Ya Wang[1], Yen-Hsyang Chu[2, *], Ching-Lun Su[2], Ruey-Ming Kuong[2], Hsyang-Chan Chen[2], and Fan-Da Chu[3]

[1] *Department of Physics, Chinese Culture University, Taipei, Taiwan, ROC*
[2] *Institute of Space Science, National Central University, Chung-Li, Taiwan, ROC*
[3] *Telecommunication Laboratory, Chung-Wha Telecommunication Company, Chung-Li, Taiwan, ROC*

Received 30 April 2007, accepted 22 January 2008

ABSTRACT

In this article, we present an electron density profile retrieved from total electron density estimated from the difference in phase path excess between GPS frequencies L1 and L2 measured by the FORMOSAT-3/COSMIC satellite, in which the radio occultation inversion technique is employed for retrieval. Except for a regular F layer peak located at a height of about 290 km and a minor peak centered at a height of 140 km, a pronounced sporadic E layer was observed at a height of about 105 km. This intense electron density layer with thickness of about 10 km has very sharp boundaries on the top and bottom sides with scale lengths of -22 and 13 km, respectively. At the time when COSMIC GPS radio occultation took place in the vicinity of Taiwan, the Chung-Li 30 MHz coherent radar detected strong backscatter from 5-meter plasma irregularities. The peak radar backscatter is situated at a height of about 110 km in the topside of the Es layer with a very steep electron density gradient. Interferometry measurement made by the four separate and independent receiving channels of the Chung-Li 30 MHz radar indicates that the configuration of the large scale plasma structure constituted by 5-meter scale field-aligned irregularities is patch-like, and a 2-minute oscillation in zonal displacement of the plasma structure was found. From the temporal displacement of the echo patterns from the plasma irregularities in the bottom side of the layer, the plasma structure in the bottom side of the Es layer was found to move westward at a trace velocity of about 6.2 m s^{-1}. The exceedingly small drift velocity combined with the relatively large scale length of the electron density gradient seem to suggest that the 5-meter plasma irregularities are very unlikely generated through the non-linear cascade process of the large plasma structure at kilometer scale induced by gradient drift instability. Moreover, in light of the fact that both the observed drift velocity (less than 15 m s^{-1}) of the kilometer-meter scale plasma wave and the measured Doppler velocity (about 50 m s^{-1}) of the 5-m plasma irregularities are much smaller than the 280 m s^{-1} that is required to directly excite plasma waves through gradient drift instability, it suggests that the 5-m plasma irregularities observed by the Chung-Li 30 MHz radar are very unlikely the result of direct excitation through gradient drift instability.

Key words: Chung-Li 30 MHz radar, Field-aligned irregularities, Gradient drift instability

Citation: Wang, C. Y., Y. H. Chu, C. L. Su, R. M. Kuong, H. C. Chen, and F. D. Chu, 2009: Campaign investigation of ionospheric plasma irregularities in sporadic E region using FORMOSAT-3/COSMIC satellite and Chung-Li 30 MHz coherent radar. Terr. Atmos. Ocean. Sci., 20, 237-250, doi: 10.3319/TAO.2008.01.22.01(F3C)

1. INTRODUCTION

The GPS radio occultation inversion technique based on the Abel transformation has been shown to be an effective method for retrieving the ionospheric electron density profile from the bending angle of a GPS ray that is measured by a GPS receiver on board a low orbit satellite receiving GPS signals propagating through the ionosphere (Schriner et al. 1999; Hajj et al. 2000). The accuracy and precision of the radio-occultated electron density have been validated in terms of ground-based radar measurements, including

* *Corresponding author*
E-mail: yhchu@jupiter.ss.ncu.edu.tw

ionosonde and incoherent scatter radar (ISR) (Hajj and Romans 1998; Tsai et al. 2001; Stolle et al. 2004). Nevertheless, most of the ionospheric studies based on the radio-occultated electron density data were concentrated on the main body of the ionosphere, namely, the F region (Hajj et al. 2000; Straus 2007), and only very limited investigations on the ionospheric E region have been carried out and reported. For example, Hocke and Tsuda (2001) analyzed sporadic E layer data observed by MicroLab-1 satellite to study the connection between gravity wave activity occurring in the lower atmosphere and the occurrence of the sporadic layer. Hernandez-Pajares et al. (2000) compared GPS occultation-retrieved foE and ionosonde-measured foE and found that they are in general agreement. Hocke and Igarashi (2002) compared peak electron densities of the sporadic E (Es) layer at noon retrieved by GPS/MET satellite with those measured by ionosondes distributed in eastern Asia and found that they are in general agreement with each other. Tsuda and Hocke (2004) analyzed GPS radio occultation data obtained by the GPS/MET (GPS/Meteorology) experiment to study the wave effects on the plasma irregularities in ionospheric sporadic E region. Luhr et al. (2004) made use of the data collected by magnetometer and Planar Langmuir Probe (PLP) on board CHAMP satellite to investigate the global behavior of equatorial electro-jet in ionospheric E region.

It is noteworthy that the height variation of the radio-occultated electron density is particularly susceptible to the intense plasma irregularities and the steep vertical gradient of the electron density. The electron density profile will be highly fluctuated and severely distorted when the plasma irregularities and/or the steep electron density gradient appear in the propagation path of the GPS ray (Hajj and Romans 1998). However, if the plasma irregularities are not strong and the electron density gradient is not sharp, it is expected that radio occultation inversion of the electron density profile will be possible. In this article, the electron density profile retrieved by using the radio occultation technique with the FORMOSAT-3/COSMIC satellite in combination with the backscatter from 5-m scale plasma irregularities observed by the ground-based Chung-Li 30 MHz coherent radar are employed to investigate the plasma irregularities in the Es layer. We find that the radar backscatter primarily occurred in the top and bottom side of the Es layer with sharp electron density gradients. In addition, interferometry measurements show that the plasma irregularities moved westward at a very low speed about 6.2 m s^{-1}. This article is organized as follow. In section 2, the radio-occultated electron density profile will be presented. In addition to the characteristics of the Chung-Li 30 MHz coherent radar, the backscatter and the Doppler spectra of the 5-meter plasma irregularities measured by the radar will be introduced and presented in section 3. The interferometry measurement of the plasma irregularities will be presented in section 4. The discussion and the conclusion will be given in section 5.

2. COSMIC-MEASURED ELECTRON DENSITY PROFILE

According to the principle of radio occultation inversion, the height variation of ionospheric refractivity can be retrieved from the measured bending angle of a GPS ray by using the Abel integral transform and then obtain the electron density profile by converting the refractivity into electron density in accordance with the Appleton relation (Rishbeth and Garriott 1969; Kursinski et al. 2000). Alternatively, on the basis of the Abel transform, it can be shown that the ionospheric electron density profile can be inverted directly from calibrated total electron content (TEC) measured by the GPS receiver on board the COSMIC satellite (Schreiner et al. 1999). The relation between electron density and TEC is given by:

$$n_e(r) = -\frac{1}{\pi}\int_{r}^{r_{LEO}} \frac{dTEC/dr_1}{\sqrt{r_1^2 - r^2}}\, dr_1 \qquad (1)$$

where r is the radial distance at tangent point, r_{LEO} is the distance from earth center to LEO satellite, and r_1 is the impact distance of the straight line connecting GPS and LEO satellites. Note that one of the advantages of using Eq. (1) to retrieve n_e from calibrated TEC is to avoid the problem of the requirement of the refractivity (or electron density) at the LEO satellite orbit in the occultation inversion from bending angle (Schreiner et al. 1999).

Figure 1 presents the electron density profile (thick curve) measured by satellite number 2 of FORMOSAT-3 through radio occultation inversion technique, in which the calibrated total electron content (thin curve) is also depicted. Note that the duration that it takes the satellite to complete the entire occultation measurement from 800 km down to surface (with height resolution ~2.75 km) is about 16 minutes (from 23:26:24 LT to 23:42:58 LT). As shown, a striking F layer electron density peak with a maximum value of about 1.05 10^5 #/cm^3 occurred at a height of around 285 km. Moreover, there are two peaks with comparable electron density located at heights around 140 and 105 km in ionospheric E region, respectively. The former is characterized by a relatively smooth and broad height distribution of the electron density profile with -3 dB half-width of about 50 km. However, the latter is characterized by irregular height distribution of the electron density with very narrow thickness of about 10 km. The large discrepancies in the patterns of the electron density peaks seem to imply that the electron density structures constituting these two peaks are very different. Namely, the spatial variation of the electron density for the irregular variation of the electron density profile is ex-

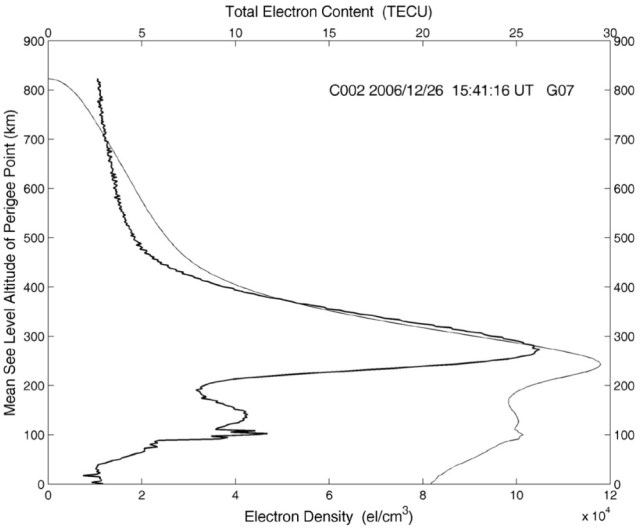

Fig. 1. The height variations of the electron density (thick curve) and total electron content (thin curve) measured by the FORMOSAT-3 satellite number 2.

pected to be much more random and fluctuated than that for the smooth and broad height distribution of the electron density profile. If the plasma irregularities responsible for the electron density peak at height around 105 km are intense enough, they will be able to be detected by a ground-based VHF coherent radar through the Bragg scattering process. In this case, the target responsible for the radar returns is the plasma irregularities at the Bragg scale, namely, the size of half of the wavelength. With the interferometry measurement made by the coherent radar, the locations of the electron density irregularities at the Bragg scale can be positioned and the dynamic behavior of the irregularities can be inferred from their Doppler velocities combined with temporal displacements in the echoing region. The experimental results made by the Chung-Li 30 MHz coherent radar will be described in next section.

3. CHUNG-LI 30 MHZ VHF RADAR – CHARACTERISTICS AND OBSERVATIONS

Under the auspice of the National Science Council of the Republic of China in Taiwan, the Chung-Li VHF radar (24.9 N, 121 E, geomagnetic latitude 13.3 N, Dip angle 35 N) was founded on the campus of the National Central University in May 1985. Originally, this radar was operated at the frequency of 52 MHz with peak transmitted power of 180 KW to remotely sense the 3-dimensional wind velocity, turbulence intensity, tropopause, raindrop terminal velocity and distribution, meteor trail, and so on. The capability of observing ionospheric plasma irregularities in Es region with interfereometry measurement was established in the Chung-Li radar in 1992. Since then, investigations of the MLT (Mesospheric and Lower Thermospheric) region by using the Chung-Li radar have become possible. For detailed characteristics of the Chung-Li 52 MHz radar for ionospheric measurement, see Wang and Chu (2001).

Supported by the National Space Organization (NSPO), a new bistatic 30 MHz radar system was constructed at the same site as the 52 MHz radar in 2002 and started to operate in 2005. The primary purpose of the 30 MHz radar is to comply with the COSMIC scientific missions to study ionospheric plasma irregularities combined with measurements made by ionosphere-related payloads on board the FORMOSAT-3 satellites, including GOX (GPS receiver), TBB (Tri-band Beacon) signals, and TIP (Tiny Ionospheric Photometer). With the capability of interferometry measurement, the location and the spatial structure of the field-aligned plasma irregularities can be accurately identified and their dynamic behavior can also be obtained from the temporal displacement of the echoing region projected on the mutually orthogonal planes. Besides COSMIC missions, in light of its transportable property, the 30 MHz radar can also be used to support other space science-related missions, such as sounding rocket experiments and global campaign observations of the space weather phenomenon.

The configuration of the entire antenna array of the Chung-Li VHF radar is shown in Fig. 2, in which monostatic 52 MHz array consists of the ionospheric array and ST (Stratosphere and Troposphere) array for the measurement of ionospheric irregularities and lower neutral atmosphere, respectively. The interferometry array is designed for detecting meteor trail and lightning strike. The transmitting and receiving arrays of the bistatic 30 MHz antenna array are also presented.

The detailed characteristics of the 30 MHz radar are listed in Table 1. Especially note from Fig. 2 that the 30 MHz transmitting antenna array is an 8 1 linear array aligned in an approximately east-west direction, and the receiving array is arranged as a square consisting of 4 Yagi antenna elements. The radiation patterns of the transmitting array are presented in Fig. 3. As shown, the gain of the 30 MHz antenna beam pattern at the boresight direction is about 17.3 dB and the -3dB half-power-half-widths are, respectively, 4 in an east-west direction and 39.3 in a north-south direction.

The radar experiment was conducted by the Chung-Li 30 MHz VHF radar for the period from 1800 - 2400 LT 26 to 0000 - 0600 LT 27 December 2006. The radar parameters were set as follows: peak transmitter power of 12 KW, inter-pulse period of 5 ms, pulse width of 104 s with 13 bits Barker code, coherent integration of 2 times, starting sampling range of 72 km and 290 range gates were recorded. The radar probing range was set from 72 to 420 km with range resolution of 1.2 km. A 256-point fast Fourier transform (FFT) algorithm was utilized to compute the Doppler spectra of the echoes. The complex normalized cross spectrum is then computed, in which eight raw spectra were taken to perform the ensemble average. Each resultant cross

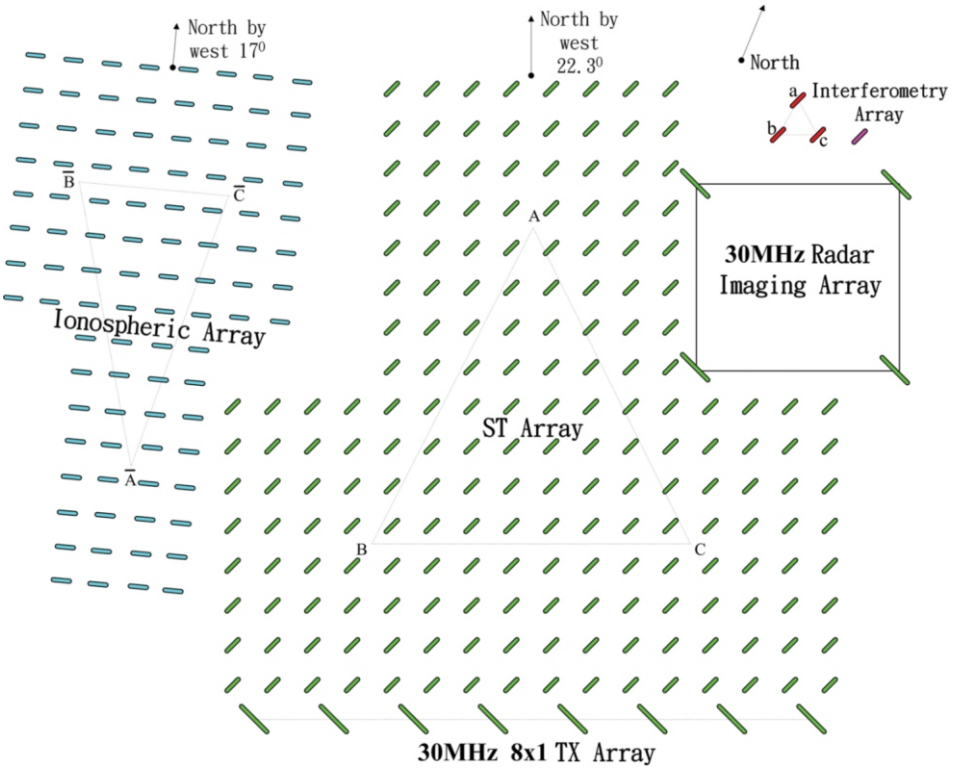

Fig. 2. Configuration of entire antenna array of the Chung-Li VHF radar.

Table 1. Characteristics of Chung-Li 30 MHz VHF radar.

Operating Frequency	30 MHz (fixed)
Type of Transmitter	Solid State
Peak Transmitted Power	12 KW
Maximum Duty Cycle	15%
Half-Power Pulse Width	1 to 200 μs (programmable)
Pulse Rise and Fall Times	200 ns minimum (programmable)
Phase Stability	max 2° over maximum pulse length
Type of Receiver	Bessel type
IF frequency	Typically 10 MHz
Noise figure	Approximate 3 dB
Receiver Bandwidth	1 MHz, 500, 250 and 125 KHz
Dynamic range	Up to approximate 67 dB
Pulse Repetition Frequency, PRF	1 Hz to 20 kHz
Digitization Resolution	16-bit
Minimum Sampling Resolution	300 meters
Number of Coherent Integrations	1 to 4096 in powers-of-two
Pulse Coding	2 to 64 bit codes, Barker or Complementary (programmable)
Number of Receiver Input Channels	4 (complex)

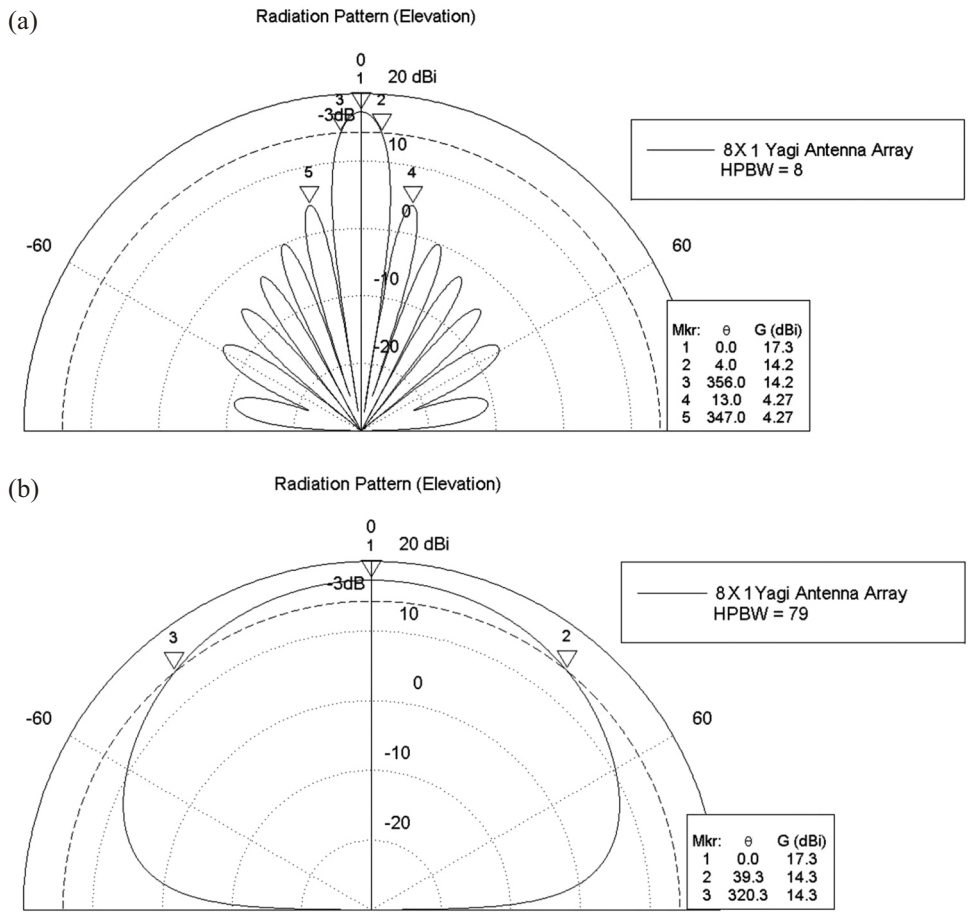

Fig. 3. Radiation patterns of the 30 MHz transmitting array. (a) pattern in east-west cross section; (b) pattern in north-south cross section.

spectrum was divided into 128 frequency bins and each bin contains 4 spectral components. The averaged phase of each bin is employed to calculate the elevation and azimuthal angles of the target in accordance with the interferometry equation shown in the next section, where the data for which the coherence is greater than 0.8 and the residue of the summation of the measured phase differences $_{31} + _{43} + _{14}$ is less than 3 are adopted for the computation.

Figure 4 is the range-time-intensity plot of the echoes from 5-meter plasma irregularities observed by the 30 MHz radar. As shown, pronounced and long-lasting radar returns occurred in the range extent from about 120 to 140 km in the time period 1800 - 2300 LT 26 December 2006. The range of the radar returns gradually decreased with time and the pattern of the echo intensity is in a form of quasi-layered structure embedded with sporadically intense backscatter. However, at around 0000 LT 27 December 2006, a clump of strong echoes (marked with A) occurred in the range extent from 140 - 150 km with duration about 35 minutes. It is noteworthy that the time when the COSMIC occultation took place to obtain the electron density profile shown in Fig. 1 is consistent with that when the echoes pattern A appeared, as indicated by the arrow. Question arises as to whether the locations of the tangent points of the GPS radio occultation are so close to the echoing region of the 5-meter plasma irregularities that the comparison between two different data sets is meaningful. Figure 5 shows the horizontal projection of the anticipated echoing region of the Chung-Li 30 MHz radar for the field-aligned irregularities in the height coverage 100 - 120 km, which is calculated from the IGRF model for an aspect angle of 0.5 and the half-power-beam-width of 4 . In addition, the projections of the tangent points of the GPS rays for the period of profiling ionopsheric electron density in the height rage 0 - 300 km from 23:43:02 to 23:45:10 LT are also presented. As shown, the horizontal separation between these two projections is about 195 km. Therefore, for the present case, the COSMIC-retrieved electron density is able to be representative of the ionospheric background structure that plays a crucial role in the generation of the 5-meter field-aligned plasma irregularities responsible for the radar returns shown in Fig. 4.

Figure 6 depicts the range variation of the self-normalized Doppler spectra for the radar data taken in the period of GPS radio occultation, where the positive (negative) Doppler velocity represents the target moving away (approaching toward) the radar. It is clear from Fig. 6 that the Doppler

velocities of the 5-meter irregularities responsible for the Es echoes varied within the range between -50 and 40 m s^{-1}, in which most of them are very small and close to zero. In addition, the Doppler spectral widths defined as the second moment of the Doppler spectrum are relatively narrow (about 25 - 45 m s^{-1}) compared to the type-2 radar spectra observed by other radars (e.g., Kelley 1989; Sahr and Fejer 1996). However, calculating the ratio of spectral width to mean Doppler velocity indicates that it takes the values from 0.24 to 0.66. Moreover, the shape of the Doppler spectra presented in Fig. 6 is quasi-Gaussian, very similar to that of the type-2 radar spectra shown in the literature (Kelley 1989). Therefore, it suggests that the radar spectra presented here can be categorized into type-2.

4. PLASMA IRREGULARITIES IDENTIFICATION – INTERFEROMETRY MEASUREMENTS

The capability of the interferometry measurement is indispensable to a radar that has relatively broad antenna beam in the azimuth direction to be able to estimate the locations and the spatial distribution of the field-aligned plasma irregularities from observed Doppler spectra. The key parameter that is vital to the interferometry measurement is the phase difference (= $_j$ - $_n$) between the echoes received by a pair of antenna modules n and j, which can be estimated from the complex normalized cross spectrum (coherence) of the echoes in accordance with following expression (Farley et al. 1981).

$$S_{pq} = \frac{< V_p^*(\omega) V_q(\omega) >}{< |V_p(\omega)|^2 >^{1/2} < |V_q(\omega)|^2 >^{1/2}} = |S_{pq}(\omega)| e^{i\Delta\phi_{pq}(\omega)} \quad (2)$$

where $V_p(\omega)$ and $V_q(\omega)$ represent the complex Doppler spectra of the radar returns received by the antenna modules p and q, respectively, the asterisk indicates the complex conjugate and < > denote ensemble average. The magnitude $|S_{pq}(\omega)|$ (coherence) in Eq. (2) represents the significance of the localized target in the echoing region, while the phase $\phi_{pq}(\omega)$ of S_{pq} is the averaged phase difference between the radar echoes received by the separated antenna modules p and q. With the help of the measured phase differences $_{43}$ and $_{31}$, the elevation angle and azimuthal angle of the target can be derived as follows (Wang and Chu 2001):

$$\phi = \tan^{-1}\left[-\frac{\Delta\phi_{43} + 2\pi m + \Delta\Psi_{43}}{\Delta\phi_{31} + 2\pi l + \Delta\Psi_{31}}\right] \quad (3)$$

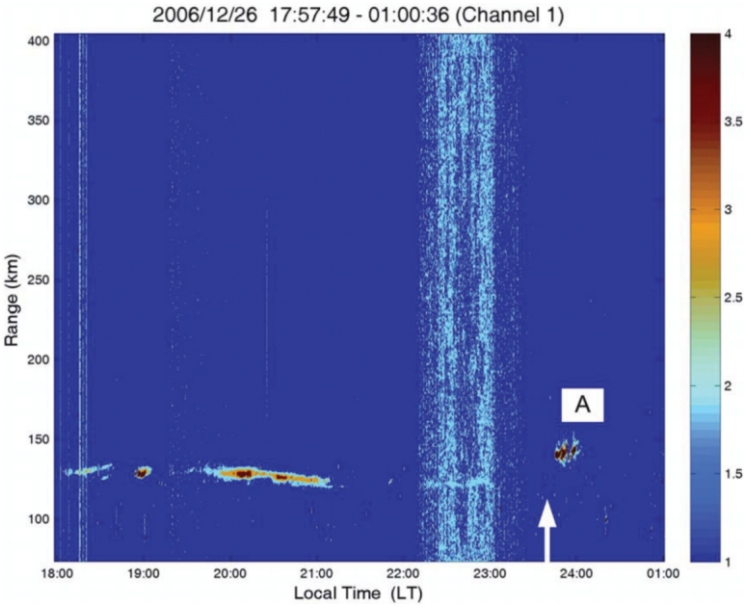

Fig. 4. Range-time-intensity of the backscatter from 5-meter field-aligned plasma irregularities observed by the 30 MHz coherent radar, in which the arrow represents the instant when the COSMIC occultation took place.

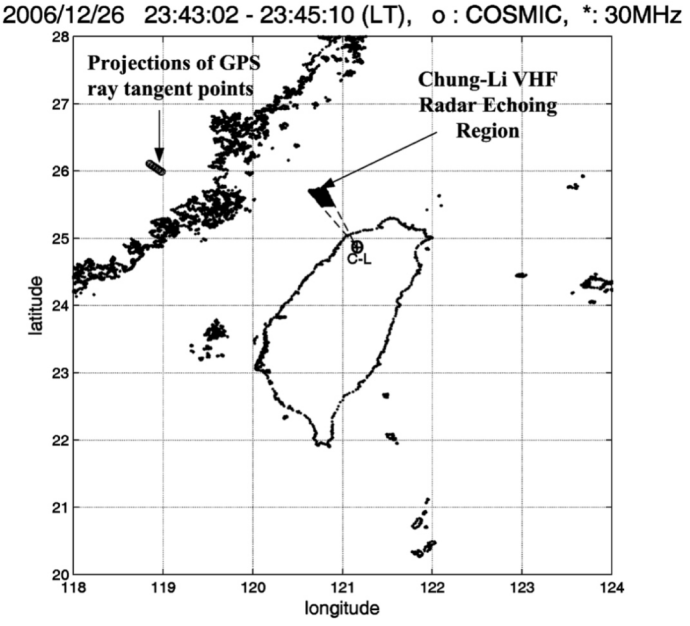

Fig. 5. Horizontal projections of the tangent points of the GPS rays for the period of profiling the height variation of the electron density in the height range 0 - 300 km from 23:43:02 to 23:45:10 LT and the anticipated echoing region of the Chung-Li 30 MHz radar for field-aligned irregularities in the height coverage 100 - 120 km, which is calculated from the IGRF model by a given aspect angle of 0.5 and half-power-beam-width of 4 .

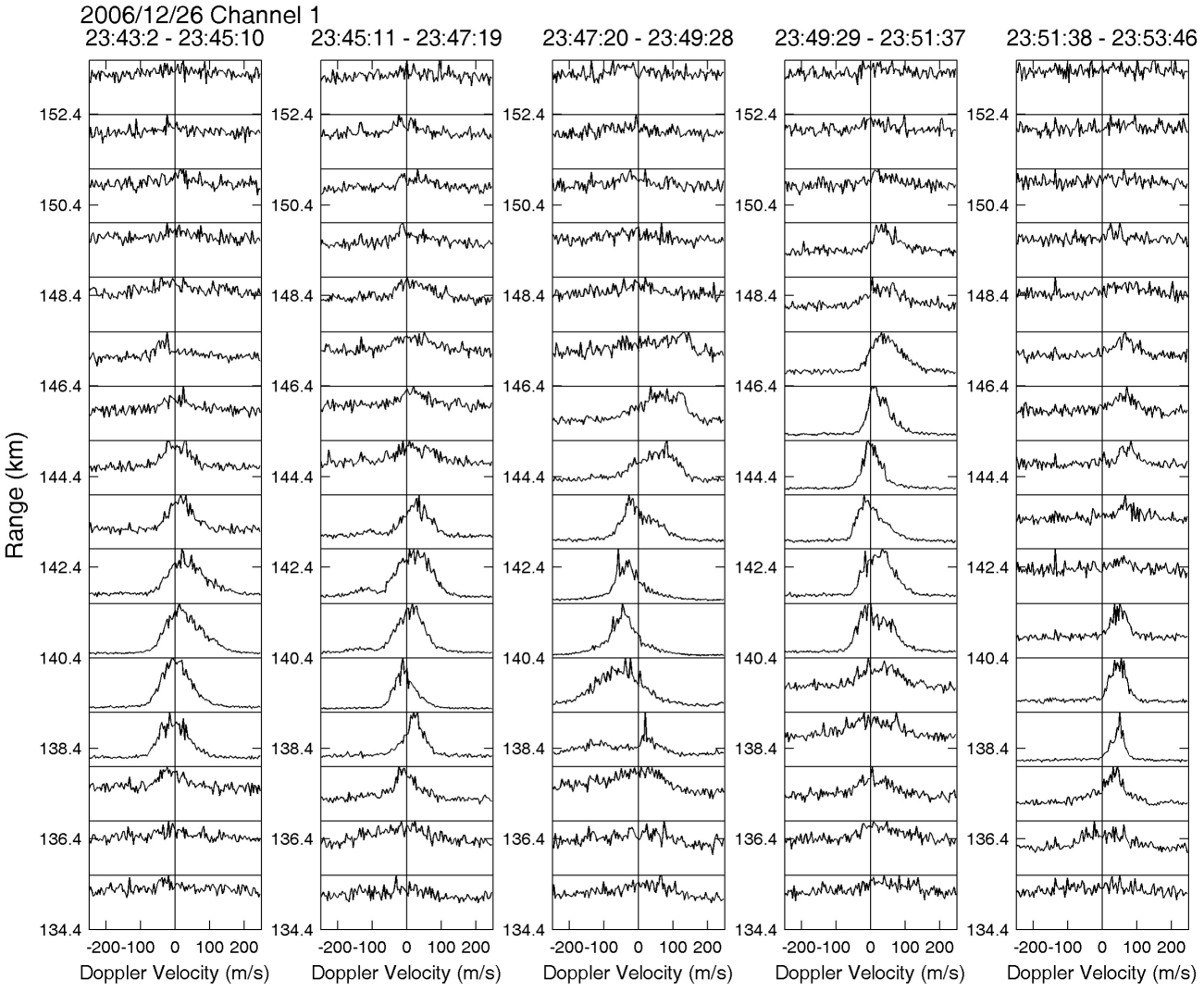

Fig. 6. Range variation of the self-normalized Doppler spectra for the radar data taken at around the time of GPS radio occultation, where the positive (negative) Doppler velocity represents the target moving away (approaching toward) the radar.

$$\theta = \cos^{-1}\left[\frac{\Delta\phi_{43} + 2\pi m + \Delta\Psi_{43}}{kd\sin\phi}\right] \quad (4)$$

where k is wavenumber, d is the distance between Yagi 1 and 3, l and m are, respectively, the interferometry lobe numbers in vertical and azimuthal directions. For the Chung-Li 30 MHz radar the values of l and m should be 1 and 0, respectively. Note that $_{43}$ and $_{31}$ in Eqs. (3) and (4) represent the system phase biases for the antenna pairs 4-3 and 3-1, respectively, which can be estimated through the regular calibration of the antenna array.

Once the true elevation and azimuthal angles of the Es irregularities in the echoing region are obtained by using interferometry technique in accordance with Eqs. (3) and (4), the spatial structure of the plasma irregularity can then be reconstructed. Figure 7 shows the consecutive variations of the spatial distributions of the measured echoing regions projected on three mutually orthogonal planes for the data with the Doppler spectra shown in Fig. 6. The panels in the top row of Fig. 7 display the locations of Es echoes projected in the vertical plane with the axes along vertical and north-south directions, where the two solid lines declining from upper right to lower left correspond to the elevation angles of 52 and 49 , respectively. The panels in the middle row of Fig. 7 display the projections of the echoes in the azimuthal planes with the axes along vertical and east-west directions, while the panels in the bottom row represent the projections of the Es echoes on the horizontal planes. The vertical straight line in each panel in the middle and bottom rows represents the projection of the apex direction of the transmitting radar beam. From the echo patterns projected on the vertical planes shown in Fig. 7, the Es echoes from 5-meter field-aligned irregularities that were distributed closely along

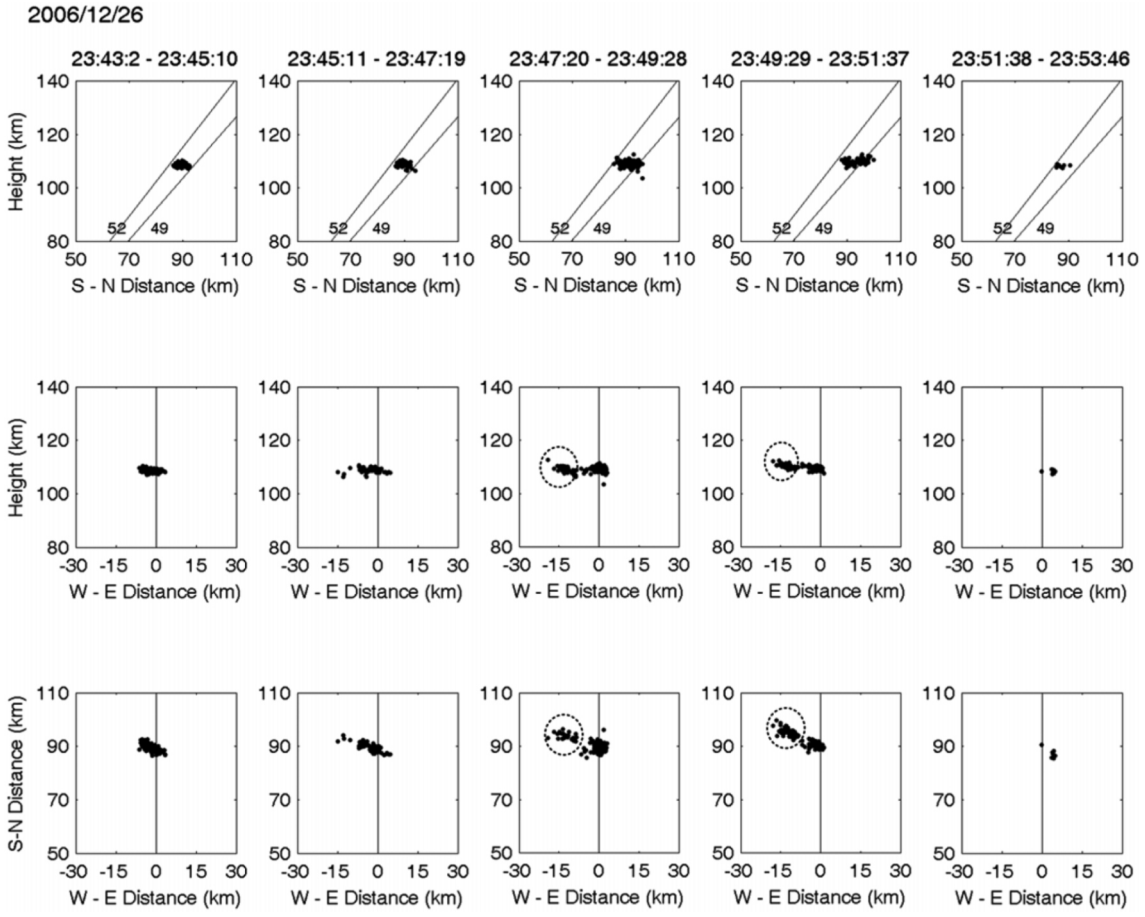

Fig. 7. Consecutive variations of the spatial distributions of the Es echoes projected on three mutually orthogonal planes, in which the dotted circle (middle and bottom panel) include the echo group in the west side of the radar beam to distinguish the echo group situated at the radar beam axis that is represented by a vertical line located at 0 in x-axis.

the line with elevation angle of 52 occurred in the height range of 105 ~ 110 km. This feature strongly suggests that the plasma irregularities responsible for the echoes have field-aligned property with exceedingly narrow aspect angle of about 0.25 (Chu and Wang 2002a).

The spatial distributions of the echoing patterns displayed on the azimuth and horizontal planes suggest that the whole plasma structure comprised two separate and individual plasma irregularity groups with a horizontal separation of about 10 km between their centers. The horizontal extents of the individual plasma irregularity groups in the zonal direction were about 10 - 15 km. Detailed examination of the temporal displacements of the plasma irregularity groups shows that they have different dynamic behaviors. The plasma irregularity group located at the radar beam axis did not displace vertically, but had slight displacement in zonal direction. However, without noticeable displacement in the horizontal direction, the group located in the west side of the radar beam moved upward consistently at a velocity of about 27 m s^{-1}. The different movements in combination with the relatively small separation between these two plasma irregularity groups suggest that physical factors governing the dynamic behaviors of these two groups are very different and need to be investigated in more detail.

Inspecting the temporal variation of the Doppler spectra in the ranges 139.2 - 141.6 km, shown in Fig. 6 denotes that there seem to be quasi-periodic oscillations in the Doppler velocities. Moreover, in the same period, the averaged position of the plasma irregularity group located at the antenna beam axis displayed in the bottom panels of Fig. 7 also shows a corresponding oscillation in the zonal displacement. In order to find out the detailed characteristics of these oscillations and their connections during this period, the radar data taken at higher time resolution are re-analyzed. Figure 8 demonstrates 2-minute oscillations in Doppler velocities and zonal displacements of the kilometer-scale plasma structures for the heights 139.2, 140.4, and 141.6 km, respectively, in which the time resolution for each data point is 6.4 sec. The amplitudes of the Doppler velocity and zonal displacement oscillations are, respectively, about -30 - 50 m s^{-1} and -7 ~ +1 km. It is clear from Fig. 8 that a nearly 90 phase shift between the oscillations of the Doppler velocity and the zonal displacement

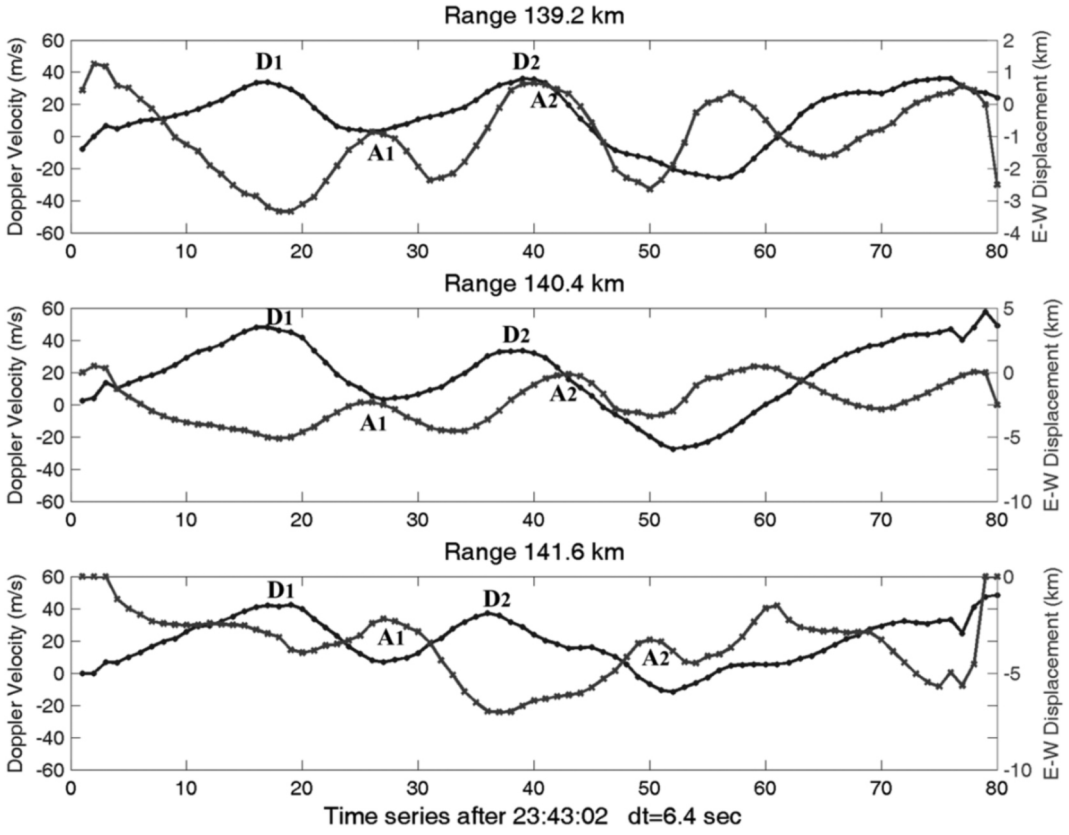

Fig. 8. Time series of 2-minute oscillations in Doppler velocities (blue curve) and zonal displacements (green curve with cross) of the kilometer-scale plasma structures for the heights 139.2, 140.4, and 141.6 km, respectively, in which the time resolution of each data point is 6.4 sec.

of the plasma structure is observed. It is noteworthy that the Doppler velocity that we observe is the result of the radial velocity of 5-meter field-aligned irregularities. Therefore, a 90 phase shift between the oscillations of the Doppler velocity and the zonal displacement seems to suggest that the meter-scale field-aligned irregularities are frozen in the kilometer scale plasma structure. In fact, this phenomenon has also been observed for the plasma irregularities responsible for the quasi-periodic echoes (Chu et al. 2007a). We will discuss in the next section the physical process involved in the generation of this 2-minute oscillation in the plasma irregularities.

If the electron density profile retrieved by the COSMIC measurement can be representative of the vertical structure of the background ionosphere, the physical processes responsible for the generation of the 5-meter plasma irregularities occurring in the top and bottom sides of the Es layer can be explored. Figure 9 compares the height variations of the COSMIC-retrieved electron density (dotted curve) for the period 23:43:02 - 23:51:37 LT with the averaged echo intensities from 5-meter field-aligned plasma irregularities (solid curve) in the height range 95 - 112 km for different periods. As indicated, the peak of the radar backscatter from the plasma irregularities in the period 23:43:02 - 23:51:37 LT is situated in the top side of the Es layer where the electron

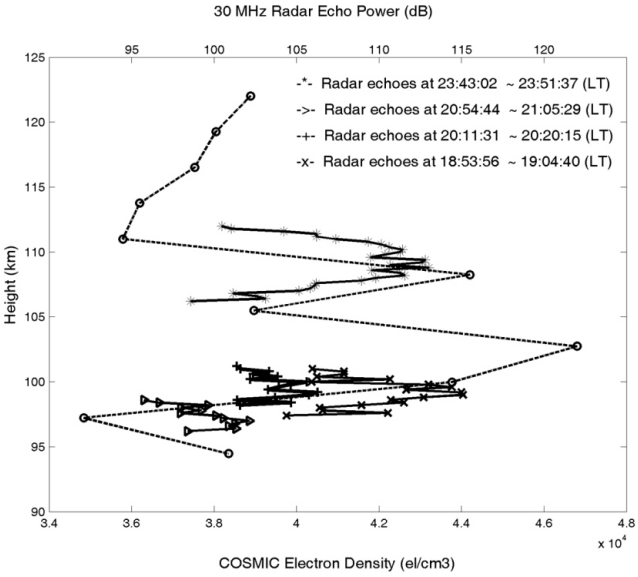

Fig. 9. Height variations of the COSMIC-retrieved electron density (dotted curve) for the period 23:43:02 - 23:51:37 LT and the averaged echo intensities from 5-meter field-aligned plasma irregularities (solid curve) in the height range 95 - 112 km for different periods.

density gradient is maximum. Similarly, the radar echoes from the 5-m plasma irregularities in the periods 18:53:56 - 19:04:40 LT, 20:11-20:20 LT, and 20:54-21:05 LT occurred in the height range 97 - 103 km in the bottom side of the Es layer with sharp and positive electron density gradient. Figure 10 shows the vertical scale length L_N of the ionopsheric structure estimated from the COSMIC-measured electron density profile as shown in Fig. 1, which is defined as:

$$L_N = k_\perp BN / [\vec{k} \cdot (\nabla N \times \vec{B})] \quad (5)$$

where k is the wavenumber of the plasma waves (or irregularities), N is the vertical gradient of electron density, B is magnetic field, and k is component of wavevector $\vec{k}$ perpendicular to magnetic field B. The data shown in Fig. 10 are calculated in accordance with Eq. (5) under the assumption of $\vec{k}$ // (N $\vec{B}$). As indicated in Fig. 10, the scale lengths at heights 98 and 110 km are approximately 13 and -22 km, respectively, where the peaks of radar echo powers occurred.

As shown in Fig. 6, from relatively small Doppler velocity and broad spectral width, the targets responsible for the Doppler spectra were the type 2 plasma irregularities. It is generally thought that the mechanism involved in the generation of the type 2 meter-scale plasma irregularities in the Es region is gradient drift instability through the nonlinear cascade process (Fejer et al. 1984; Farley 1985). The linear growth rate of gradient drift instability has the following vector form (Woodman et al. 1991).

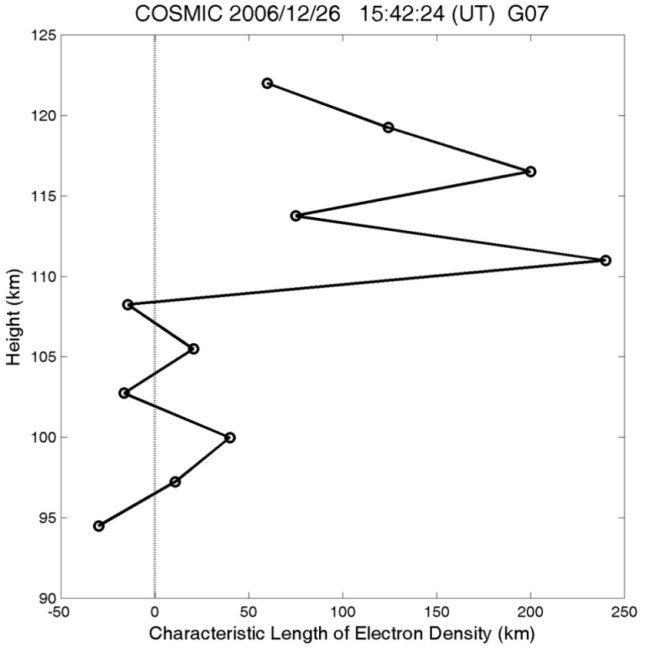

Fig. 10. Vertical scale length of the ionopsheric structure estimated from the COSMIC-measured electron density profile as shown in Fig. 1.

$$\gamma \propto \frac{1}{1 + \psi} \vec{k} \cdot \vec{V_D} (\vec{k} \cdot \nabla N \times \vec{B}) \quad (6)$$

where

$$\psi = \frac{\nu_e \nu_i}{\Omega_e \Omega_i} (1 + \frac{\Omega_e^2}{\nu_e^2} \sin^2 \phi) \quad (7)$$

where ν_i and ν_e are, respectively, the ion-neutral and electron-neutral collision frequencies, $_i$ and $_e$ are, respectively, the ion and electron gyro-frequencies, V_D is the relative electron-ion drift velocity that is driven by **E** **B** drift effect, and ϕ is magnetic aspect angle with respect to perpendicularity to the magnetic field line. Therefore, for the plasma irregularities located in the bottom side of Es layer, the excitation of the gradient drift instability requires upward/northward pointed electric field and westward drift of the irregularities such that we have $\vec{k} \cdot \vec{V_D} > 0$ and $\vec{k}$ N $\vec{B} > 0$. Moreover, linear theory also predicts that, by including the ion drift velocity Vi, the threshold velocity V_{th} for the direct excitation of unstable waves can be expressed as follows (Fejer et al. 1984; Chu and Wang 2002b).

$$V_{th} = C_s (1 + \Psi) \left(\sqrt{Q^2 + P^2 + 1} - Q \right) \quad (8)$$

where

$$V_{th} = (V_D + \Psi V_i)_{th} \cos\theta \quad (9)$$

and

$$Q = \frac{\nu_i^2}{2\Psi k^2 C_s L_N \Omega_i} \quad (10)$$

$$P = \frac{2\alpha N_o \nu_i (1 + \psi)}{k^2 C_s^2 \psi} \quad (11)$$

In the above expressions, is the cone angle for the excitation of unstable waves and = 0 if the wave vector is parallel to the vector sum $\vec{V}_e$ $\psi \vec{V}_i$, C_s (= $\sqrt{K(T_e \quad T_i)/m_i}$) is ion-acoustic wave speed, m_i is the mean ionic mass in unit of amu, is recombination coefficient, N_o is mean electron density, and K (= 1.38 10^{-23} Joules/molecular K) is Boltzmann's constant. Figure 11 depicts the time sequences of the zonal displacements of the echo patterns projected on the azimuth planes (the ordinate indicates height and abscissa east-west direction) for the periods 18:56:05 - 19:06:49 LT and 20:00:45 - 20:11:30 LT, respectively. As shown, the av-

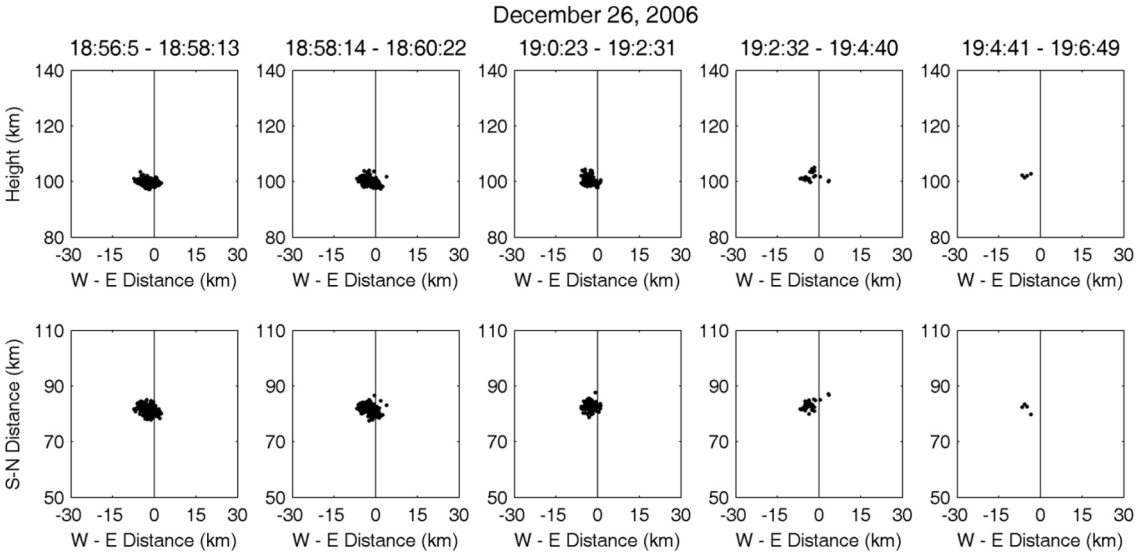

Fig. 11. Time histories of the echo patterns projected on the azimuth planes for the periods 18:56:05 - 19:06:49 LT and 20:00:45 - 20:11:30 LT. As shown, the plasma structure moved from east to west at a velocity of about 6.2 m s^{-1}.

eraged trace velocity estimated from the temporal displacements of the echo patterns is very small, only approximately 6.2 m s^{-1} westward. This exceedingly small drift velocity combined with large scale length (approximately 13 km) of the electron density gradient make it almost impossible to excite gradient drift instability. This is because in this condition the threshold velocity for directly exciting 10 km irregularity size by the gradient drift velocity is about 30 m s^{-1} (Fejer et al. 1984), where the following parameter are used in the calculation: ion-acoustic wave speed ~ 325 m s^{-1}, $_i$ ~ 4.6 10^3 s^{-1}, $_e$ ~ 4.7 10^4 s^{-1}, $_i$ ~ 180 s^{-1}, $_e$ ~ 10^7 s^{-1}, ψ ~ 10^3 - 10^4 s^{-1}, and 2 N_o ~ 0.06 s^{-1}, where is recombination coefficient, N_o is mean electron density (Rishbeth and Garriott 1969; Kelley 1989). With the same parameters, we can calculate the dependence of V_{th} on wavelength and scale length as shown in Fig. 12, in which the variations of the threshold velocity with the unstable wavelength (or irregularity size) along with the scale length of the electron density profile L_N are shown. A positive (negative) value in L_N represents an upward (downward) electron density gradient. As indicated, for 5-m unstable wave (or irregularity) with L_N = 5 km, the threshold velocity is approximately 80% of the ionic acoustic wave speed (Cs) that is about 360 m s^{-1} in nighttime Es region. In light of the fact that the observed drift velocity (less than 15 m s^{-1}) of the kilometer-meter scale plasma wave and the measured Doppler velocity (about 50 m s^{-1}) of the 5-m plasma irregularities are much smaller than the about 280 m s^{-1} that is required to directly excite the plasma waves through gradient drift instability, it suggests that the 5-m plasma irregularities observed by the Chung-Li 30 MHz radar are very unlikely the result of direct excitation through gradient drift instability.

Except for gradient drift instability, type 2 field-aligned irregularities at meter scale may be induced by neutral turbulences in the Es region that are generated through dynamic instability and/or convective instability associated with the gravity wave breaking (Gurevich et al. 1997; Bishop et al. 2004; Chu et al. 2007b). In the next section, we will discuss the plausible mechanism responsible for the generation of the Es plasma irregularities observed by the 30 MHz coherent radar.

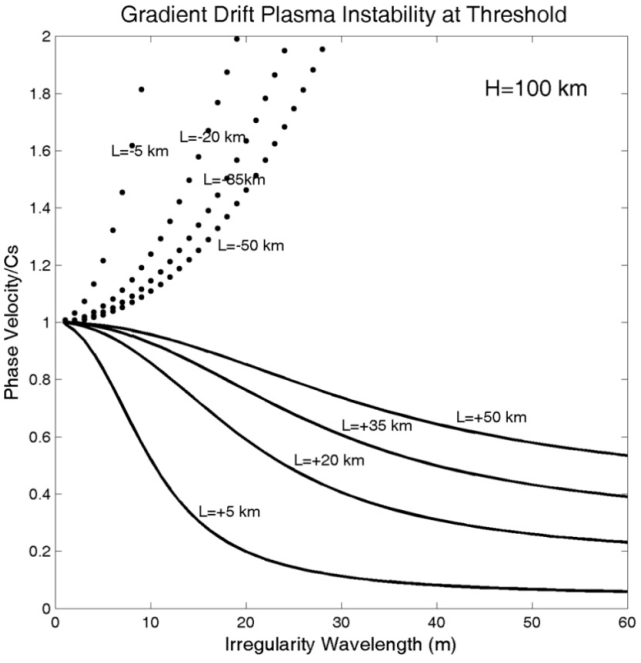

Fig. 12. Threshold velocity for the excitation of an unstable wave at different wavelengths through gradient-drift instability, where Cs is the ionic acoustic wave speed.

5. DISCUSSION AND CONCLUSION

It is well recognized that the ionospheric electron density structure in Es region is very complicated, which is characterized by intense electron density layer with sharp boundaries and salient plasma irregularities inside the layer (Rishbeth and Garriott 1969). This feature not only can cause the degradation of the accuracy of the radio occultation inversion of the electron density profile due to invalid assumption of spherical symmetry, but also may give rise to multiple path propagation. Note that multipath effect occurs when strong refractivity gradients are present. Analysis of the GPS/MET data has indicated that this situation is a common feature rather than an exception (Hajj et al. 1998). However, in the conditions that the plasma irregularities are not strong and the electron density gradient is not steep, it is expected that the height variation of the electron density will be only slightly disturbed and the background ionosphere structure is still discernible. In fact, we can employ the height distribution of the radar backscatter from the electron density fluctuations at Bragg scale to verify the locations of the sharp boundaries of the electron density layer retrieved by radio occultation technique. This is because, if the fluctuations of the electron density are generated through the plasma turbulence mixing process, the variance of the electron density fluctuations will be proportional to the gradient of the background electron density (Farley 1985). Namely, the sharper the electron density gradient is, the larger the variance of the electron density fluctuations will be. We also note that radar backscatter is proportional to the variance of the electron density fluctuations, peak radar backscatter is therefore expected to occur at the place where the gradient of the electron density is maximum. This assertion has been shown by the experimental results presented in Fig. 9.

Because of the extremely small aspect angle of the 5-meter field-aligned irregularities, it is expected that the width of the expected echoing region in the meridional direction resolved by the interferometry technique will be exceedingly narrow, only about 4 - 5 km for the present case. However, the resolvable dimension of the anticipated echoing region in the zonal direction may be as large as 20 km or more, depending on the strength of the 5-meter plasma irregularities in the antenna beam. In this situation, only a small portion of the large scale plasma structure can be seen by the 30 MHz coherent radar if the horizontal dimension of the plasma structure is greater than the resolvable dimension of the expected echoing region. Therefore, the trace velocity estimated from the temporal displacement of the echo pattern may not be the true velocity of the plasma structure (Chu et al. 2007a). If the true drift velocity of the plasma irregularities is greater than the threshold velocity for exciting the gradient drift instability, one might expect that meter-scale plasma irregularities can be generated through the nonlinear turbulence cascade process from the primary kilometer-scale plasma structure that is directly excited by gradient drift instability (Fejer et al. 1984, Farley 1985). However, for the present case, because of exceedingly small trace and mean Doppler velocities combined with the frozen-in property of the 5-meter field-aligned irregularities, we believe that the true velocity is very likely as low as the trace velocity (Chu et al. 2007a).

Except for **E** **B** effect, another possibility of generating small scale plasma irregularities in Es region is the neutral wind effect (Kagan and Kelley 1998). In this case, the oscillation frequency of the unstable wave excited through gradient drift instability in the rest frame is (Fejer et al. 1984):

$$\omega_r = \frac{\vec{k} \cdot (\vec{V_e} + \psi \vec{V_i})}{1 + \psi} \tag{12}$$

where V_e is the electron velocity and primarily caused by **E** **B** effect. For neutral-driven unstable waves (or irregularities) in nighttime Es region, it is reasonable to assume that the ion velocity V_i is approximate to the neutral wind velocity U due to $_i$ $_i$. Because $\psi << 1$, from Eq. (12) the phase velocity of the unstable wave is expected to be dominated by V_e, rather than U (or V_i). Linear theory shows that the unstable region where the plasma irregularities are generated will be in the top side (bottom side) of the Es layer if the neutral wind is in a west (east) direction (Kagan and Kelley 1998). From Figs. 7 and 9, the averaged drift velocity of the plasma structure that was assembled by the 5-m field-aligned irregularities and occurred in the top side of the Es layer was primarily westward. This feature is consistent with the prediction of the neutral wind-driven mechanism. Therefore, it suggests that the neutral wind-driven process that is likely responsible for the generation of the 5-m plasma irregularities presented in this study is a plausible mechanism and cannot be ruled out.

As presented in Fig. 6, the quasi-periodic variations in the Doppler velocity are observed in the range extent from 139 to 144 km (corresponding to a height extent of about 106 - 109 km). This feature seems to imply that the 5-meter plasma irregularities responsible for the echoes are undergoing a wave-like displacement that is very likely the result of the oscillation of a plasma wave with a period of about 2 minutes. Moreover, from the temporal displacements of the echoing regions projected on the vertical planes shown in Fig. 7, the plasma structures reveal a similar quasi-periodic displacement in the zonal direction. However, probably because of the limitation of the exceedingly narrow range of the expected echoing region in the meridional direction, we do not find such oscillation in the meridional displacement of the plasma structures. Note that, on the basis of the MSIS-90 model, the typical Brunt-Vaisala frequency in the height range of the Es layer is about 0.025 - 0.029 rad s^{-1},

corresponding to the period range from about 3.5 to 4.2 minutes (Chu et al. 2007b). Therefore, this 2-minute oscillation in the plasma structure seems to be unlikely induced by the Brunt-Vaisala frequency of the neutral atmosphere. Because of this, we speculate that the physical factor dominating the zonal drift of the plasma irregularities is very likely the electric field pointed in the geomagnetically meridional direction. In view of the relatively narrow extent (only a few kilometers) of the plasma structure in the zonal direction, the electric field in the plasma wave causing the quasi-periodic oscillation of the plasma irregularities in the zonal direction through the **E** **B** drift effect seems not to be resulted to the mapping of the polarization electric field originating in the F region down to Es region along the magnetic fields line (Farley 1959). Therefore, it appears that the electric field associated with the plasma wave with a period of 2 minutes was generated locally through a certain as yet unrecognized process.

Interferometry measurements presented in Fig. 7 have shown that the 5-meter field-aligned plasma irregularities responsible for the radar returns are distributed in a region with horizontal extent of about 15 - 20 km and vertical thickness of about 3 - 5 km. Notice that the configuration of the echoing region in the thin layered structure observed by a fan-like effective antenna beam (defined as the product of the physical antenna beam pattern and the aspect sensitivity of the backscatter from field-aligned irregularities) is in a striation pattern that is very narrow in meridional and widely extended in the zonal directions (Chu and Wang 2002a, 2003). Consequently, the projection of the echo region on the horizontal plane is still in a form of striation and its location will be dependent on the altitude of the layer structure (Chu and Wang 1999; Wang and Chu 2001). Namely, the higher the layered structure is, the farther from the radar in the meridional direction the echo pattern will be. This connection explains the interrelation between the positions of the echo patterns on azimuth and horizontal planes for the plasma irregularity group located in the west side of the antenna beam axis included in the dotted circle of Fig. 7, this has a tendency to move upward.

In summary, the COSMIC-retrieved electron density profile and the concurrent Es plasma irregularities measured by the Chung-Li 30 MHz coherent radar are presented in this article, in which a pronounced Es layer with thickness of about 10 km centered at height of 105 km was clearly observed. Interferometry measurements show that the plasma structures are in a patchy shape with very narrow thickness (about 3 - 5 km) in vertical and relatively wide extent (about 8 - 12 km) in zonal directions. We find that, in light of the considerably low drift velocity of the large scale plasma structure (less than 1/50 of the nominal ion-acoustic wave speed) and relatively large scale length of the electron density gradient (about 10 - 25 km), the 5-meter plasma irregularities occurring at the top and bottom sides of the Es layer seem to be unlikely generated by the non-linear cascade process from the primary kilometer scale plasma structure excited by the gradient drift instability. A more detailed examining of the dynamic behavior of the 5-meter field-aligned irregularities shows that there was a plasma wave with period about 2 minutes governing the zonal oscillation of the plasma irregularity group, in which the 5-meter small scale plasma irregularities were embedded and frozen. This feature cannot be explained by the neutral-induced plasma irregularities. These results suggest that there is still room for the development of a more appropriate theoretical mechanism to account for the findings presented in this article.

Acknowledgement This work was supported by the National Space Organization of the Republic of China in Taiwan under grant 95-NSPO(B)-RS3-FA07-02-C.

REFERENCES

Bishop, R. L., M. F. Larsen, J. H. Hecht, A. Z. Liu, and C. S. Gardner, 2004: TOMEX: Mesospheric and lower thermospheric diffusivities and instability layers. *J. Geophys. Res*., **109**, D02S03, doi: 10.1029/2002JD003079. [Link]

Chu, Y. H. and C. Y. Wang, 1999: Interferometry investigations of VHF backscatter from plasma irregularity patches in nighttime E region using Chung-Li VHF radar. *J. Geophys. Res*., **104**, 2621-2631. [Link]

Chu, Y. H. and C. Y. Wang, 2002a: Plasma Structures of 3-meter Type 1 and Type 2 Irregularities in Nighttime Mid-latitude Sporadic E Region. *J. Geophys. Res*., **107**, A12, 1447, doi: 10.1029/2002JA009318. [Link]

Chu, Y. H. and C. Y. Wang, 2002b: Three-dimensional spatial structures of mid-latitude type 1 Es irregularities. *J. Geophys. Res*., **107**, A8, 1182, doi: 10.1029/2001JA000215. [Link]

Chu, Y. H. and C. Y. Wang, 2003: Radial velocity and doppler spectral width of echoes from field-aligned irregularities localized in the sporadic E region. *J. Geophys. Res*., **108**, A7, 1282, doi: 10.1029/2002JA009661. [Link]

Chu, Y. H., C. Y. Wang, and K. F. Yang, 2007a: Plasma structures responsible for sporadic E region quasi-periodic echoes. *J. Atmos. Sol.-Terr. Phys*., **69**, 537-551, doi: 10.1016/ j.jastp.2006.10.006. [Link]

Chu, Y. H., C. L. Su, M. F. Larsen, and C. K. Chao, 2007b: First measurements of neutral wind and turbulence in the mesosphere and lower thermosphere over Taiwan with a chemical release experiment. *J. Geophys. Res*., **112**, A02301, doi: 10.1029/2005JA011560. [Link]

Farley, D. T., 1959: A theory of electrostatic field in a horizontally stratified ionosphere subject to a vertical magnetic field. *J. Geophys. Res*., **64**, 1225-1233, doi: 10.1029/JZ 064i009p01225. [Link]

Farley, D. T., 1985: Theory of equatorial electrojet plasma waves: new developments and current status. *J. Atmos. Terr. Phys*., **47**, 729-744, doi: 10.1016/0021-9169(85) 90050-9. [Link]

Farley, D. T., H. M. Ierkie, and B. G. Fejer, 1981: Radar Interferometry: A new technique for studying plasma turbulence in the ionosphere. *J. Geophys. Res*., **86**, 1467-1472, doi: 10.1029/JA086iA03p01467. [Link]

Fejer, B. G., J. Providakes, and D. T. Farley, 1984: Theory of plasma waves in the auroral E region. *J. Geophys. Res*., **89**, 7487-7494, doi: 10.1029/JA089iA09p07487. [Link]

Gurevich, A. V., N. D. Borisov, and K. P. Zybin, 1997: Ionospheric turbulence induced in the lower part of the E region by the turbulence of the neutral atmosphere. *J. Goephys. Res*., **102**, 379-388, doi: 10.1029/96JA00163. [Link]

Hajj, G. A. and L. J. Romans, 1998: Ionospheric electron density profile obtained with Global Positioning System: Results from GPS/MET experiment. *Radio Sci*., **33**, 175-190, doi: 10.1029/97RS03183. [Link]

Hajj, G. A., L. C. Lee, X. Pi, L. J. Romans, W. S. Schreiner, P. R. Straus, and C. Wang, 2000: COSMIC GPS ionospheric sensing and space weather. *Terr. Atmos. Ocean. Sci*., **11**, 235-272.

Hernandez-Pajares, M., J. M. Juan, and J. Sanz, 2000: Improving the Abel inversion by adding ground GPS data to LEO radio occultations in ionospheric sounding. *Geophys. Res. Lett*., **27**, 2473-2476, doi: 10.1029/2000GL000032. [Link]

Hocke, K. and T. Tsuda, 2001: Gravity waves and ionospheric irregularities over tropical convection zones observed by GPS/MET radio occultation. *Geophys. Res. Lett*., **28**, 2815-2818, doi: 10.1029/2001GL013076. [Link]

Hocke, K. and K. Igarashi, 2002: Structure of the Earth's lower ionosphere observed by GPS/MET radio occultation. *J. Geophys. Res*., **107**, A5, 1057, doi: 10.1029/2001JA 900158. [Link]

Kagan, L. M. and M. C. Kelley, 1998: A wind-driven gradient drift mechanism for midlatitude E-region ionospheric irregularities. *Geophys. Res. Lett*., **25**, 4141-4144, doi: 10.1029/1998GL900123. [Link]

Kelley, M. C., 1989: The earth's ionosphere, Academic Press, San Diego, California.

Kursinski, E. R., G. A. Hajj, S. S. Leroy, and B. Herman, 2000: The GPS radio occultation technique. *Terr. Atmos. Ocean. Sci*., **11**, 53-114.

Lühr, H., S. Maus, and M. Rother, 2004: Noon-time equatorial electrojet: Its spatial features as determined by the CHAMP satellite. *J. Geophys. Res*., **109**, A01306, doi: 10.1029/2002JA009656. [Link]

Rishbeth, H. and O. K. Garriott, 1969: Introduction to ionospheric physics, Academic, San Diego, California, 331 pp.

Sahr, J. D. and B. G. Fejer, 1996: Auroral electrojet plasma irregularity theory and experiment: A critical review of present understanding and future directions. *J. Geophys. Res*., **101**, 26893-26909, doi: 10.1029/96JA02404. [Link]

Schreiner, W. S., S. V. Sokolovskiy, C. Rocken, and D. C. Hunt, 1999: Analysis and validation of GPS/MET radio occultation data in the ionosphere. *Radio Sci*., **34**, 949-966, doi: 10.1029/1999RS900034. [Link]

Straus, P. R., 2007: Ionospheric climatology derived from GPS occultation observations made by the ionospheric occultation experiment. *Adv. Space Res*., **39**, 793-802, doi: 10.1016/j.asr.2006.08.009. [Link]

Stolle, C., N. Jakowski, K. Schlegel, and M. Rietveld, 2004: Comparison of high latitude electron density profiles obtained with the GPS radio occultation technique and EISCAT measurements. *Ann. Geophys*., **22**, 2015-2022.

Tsai, L. C., W. H. Tsai, W. S. Schreiner, F. T. Berkey, and J. Y. Liu, 2001: Comparisons of GPS/MET retrieved ionospheric electron density and ground based ionosonde data. *Earth Planets Space*, **53**, 193-205.

Tsuda, T. and K. Hocke, 2004: Application of GPS radio occultation data for studies of atmospheric waves in the middle atmosphere and ionosphere. *J. Meteorol. Soc. Jpn*., **82**, 419-426, doi: 10.2151/jmsj.2004.419. [Link]

Wang, C. Y. and Y. H. Chu, 2001: Interferometry investigations of blob-like sporadic E plasma irregularity using the Chung-Li VHF radar. *J. Atmos. Sol.-Terr. Phys*., **63**, 123-133, doi: 10.1016/S1364-6826(00)00141-3.[Link]

Woodman, R. F., M. Yamamoto, and S. Fukao, 1991: Gravuty wave modulation of gradient drift instabilities in mid-latitude sporadic E irregularities. *Geophys. Res. Lett*., **18**, 1197-1200, doi: 10.1029/91GL01159. [Link]